

● *Original Contribution***PROPERTIES OF PHANTOM TISSUELIKE POLYMETHYLPENTENE IN THE FREQUENCY RANGE 20–70 MHZ**ERNEST L. MADSEN,* MEAGAN E. DEANER,* and JAMES MEHI[†]*Department of Medical Physics, University of Wisconsin, Madison, WI; and [†]VisualSonics, Toronto, Ontario, Canada

(Received 7 January 2011; revised 12 May 2011; in final form 16 May 2011)

Abstract—Quantitative ultrasound (QUS) has been used to characterize soft tissues at ordinary abdominal ultrasound frequencies (2 to 15 MHz) and is beginning application at high frequencies (20 to 70 MHz). For example, backscatter and attenuation coefficients can be estimated *in vivo* using a reference phantom. At high frequencies, it is crucial that reverberations do not compromise the measurements. Such reverberations can occur between the phantom's scanning window and transducer components as well as within the scanning window between its surfaces. Transducers are designed to minimize reverberations between the transducer and soft tissue. Thus, the acoustic impedance of a phantom scanning window should be tissue-like; polymethylpentene (TPX) is commonly used because of its tissue-like acoustic impedance. For QUS, it is also crucial to correct for the transmission coefficient of the scanning window. Computation of the latter requires knowledge of the ultrasonic properties, *viz.*, density, speed and attenuation coefficients. This work reports values for the ultrasonic properties of two versions of TPX over the high-frequency range. One form (TPX film) is used as a scanning window on high-frequency phantoms, and at 40 MHz and 22°C was found to have an attenuation coefficient of 120 dB/cm and a propagation speed of 2093 m/s. (E-mail: elmadsen@wisc.edu) © 2011 World Federation for Ultrasound in Medicine & Biology.

Key Words: High-frequency, Phantom, Scanning window, TPX, Ultrasonic properties, Speed, Attenuation.

INTRODUCTION

Scanning windows on tissue-mimicking phantoms are often Saran Wrap (Dow Chemical Company, Midland, MI, USA) (Wear et al. 2005) or plastic-coated aluminum foil (Stiles et al. 2008). Typical thicknesses of Saran Wrap used on phantoms in our lab are 12 μm and 25 μm . At ultrasonic frequencies commonly used in abdominal imaging (2 to 15 MHz), reverberations between the scanning window and the contacting transducer are shallow enough that they generally do not compromise the usefulness of the phantom. However, at high frequencies (20 to 70 MHz) such as are used in small animal (preclinical) imaging, ophthalmology or dermatology, depths of penetration are small—a few millimeters to ~ 15 mm (Foster et al. 2000; Raju et al. 2001). For these high-frequency imagers, even a very thin 12- μm Saran Wrap window can result in reverberations that compromise the usefulness of the phantom (Madsen et al. 2010). The reverberations probably arise within

the transducer, which is fabricated of materials to avoid reflections from skin contacting the transducer.

Polymethylpentene, also known as TPX[®] (Trademark of Mitsui Chemicals America, Inc., Rye Brook, NY, USA), is a plastic known for its tissue-like low acoustic impedance and reasonably low attenuation at low frequencies (~ 1.6 dB/cm/MHz in the 2 to 12 MHz range) (Bloomfield et al. 2000). There are two versions of TPX relevant to ultrasound (US) imaging: film and sheet. The film version is made at thicknesses < 0.5 mm, whereas the sheet version is thicker (≥ 2.5 mm); the film version is the one we use on high-frequency phantoms. Also, the production process is different for the film and sheet versions; *viz.*, the film is extruded onto a cylinder and hardens without compression, whereas the sheet is extruded and then hardens under compression. We have found that scanning windows composed of TPX films cause no significant reverberations detectable in B-scans of phantoms at high frequencies (15 to 70 MHz) (Madsen et al. 2010).

Some quantitative uses of phantoms require knowledge of the transmission coefficient of the scanning window, *e.g.*, the reference phantom method for estimating the attenuation and backscatter coefficients

Address correspondence to: Ernest L. Madsen, Department of Medical Physics, 1005 WIMR, 1111 Highland Avenue, University of Wisconsin, Madison, WI. E-mail: elmadsen@wisc.edu

(Yao et al. 1990; Lu et al. 1999). The reference phantom method eliminates scanner instrumental factors, but the transmission coefficient of any scanning window on the phantom must be accounted for.

Sufficiently accurate clinical determinations of attenuation and backscatter coefficients could contribute to differentiating benign and malignant tumors. In the low-frequency range (2 to 12 MHz), the reference phantom method has been used to estimate backscatter and attenuation coefficients of liver (Lu et al. 1999), breast (Anderson et al. 2001), brain (Strowitzki et al. 2007), cervix (McFarlin et al. 2010; Labyed et al. 2011) and blood vessel plaque (Shi et al. 2007).

In the high-frequency range, the reference phantom method has been used for estimating attenuation coefficients of dermis and subcutaneous fat in the 14–50-MHz range (Raju and Srinivasan 2001). A laboratory system was used in which the reference phantom had a Saran Wrap scanning window. Reverberation interference was avoided in the 3-mm depth range interrogated by obtaining backscatter data with the transducer face in water at a distance >3 mm from the skin and phantom surfaces; a reference phantom with a well-characterized TPX scanning window would not have required a special scanning situation involving an intermediate water path.

Immediate clinical application of the reference phantom method in which the phantom has a TPX scanning window is in determination of high-frequency backscatter and attenuation coefficients in dermatology. Distinction between benign and malignant tumors may be possible.

Application of the reference phantom method at high frequencies is being pursued regarding development of an improved technique for breast tumor biopsy. Preliminary to application in patients, a reference phantom with a well-characterized TPX scanning window, produced in our lab, is currently in use over the high-frequency range (20 to 70 MHz) at the University of Illinois to characterize and differentiate *in vivo* human breast tumors grown in small animal hosts. An ultimate goal is to develop a high-frequency US needle probe for improved biopsies of human breast tumors. The probe will be inserted into the tumor and radiofrequency (RF) data taken to allow estimation of attenuation and backscatter coefficients of the tumor tissue using the reference phantom method. Transmission through a scanning window without reverberations is necessary, and that window will likely be TPX; using the results of the work reported here, accurate correction of the data to account for transmission is facilitated.

Another high-frequency reference phantom with a TPX window has been used for *in vitro* measurements of backscatter and attenuation coefficients of blood vessel plaque (McCormick 2011). Using the reference phantom in a similar way could be implemented for intravascular

ultrasound (IVUS), which involves frequencies between 20 and 50 MHz.

To characterize a material ultrasonically, the density, propagation speed and attenuation coefficients must be known over the frequency range of concern. Such characterization will allow, *e.g.*, computation of the (linear) transmission coefficient between two media. Therefore, we have measured the attenuation coefficients of TPX film from 20–70 MHz. Propagation speed was also determined and the small speed dispersion (~ 20 m/s between 20 and 70 MHz) is consistent with the Kramers-Kronig relations (O'Donnell et al. 1981). Because thicker TPX (a few mm) can be present on medical US scan heads, *e.g.*, to form lenses or to form transmission covers over mechanically scanned arrays, we also report on the speed and attenuation properties of the sheet form.

Finally, a test of the uncertainty estimates for measured propagation speeds and attenuation coefficients of TPX film was carried out by comparing directly measured transmission coefficients with those predicted using the measured values of propagation speeds and attenuation coefficients. The media separated by the TPX film were different and were representative of clinically relevant media.

METHODS AND MATERIALS

The source (distributor) of the TPX film was the C. S. Hyde Company (Lake Villa, IL, USA), and the manufacturer was Ajedum Films, a division of Solvay Solexis, Inc. (Newark, NJ, USA). Raw TPX (for making film or sheet) can be obtained in different grades, and the film we used was made from grade RT-18. The stock sheet form was about 2.4 mm thick and was made from TPX grade DX845; thinner layers of the sheet form were made by milling down sections of the 2.4-mm stock sheet. The distributor—and manufacturer—of the TPX sheet was Westlake Plastics (Lenni, PA, USA). The particular grades of TPX investigated correspond to those we have used on phantoms in our lab; for example, the TPX film has been used as a scanning window on phantoms made for performance testing at high frequencies as well as on high-frequency reference phantoms (Yao et al. 1990) currently in use in our lab and a lab at the University of Illinois-Urbana. The cost of 128- μm -thick TPX film is currently about \$7.50 per square foot.

Measurement methods

Propagation speeds and attenuation coefficients. All measurements were made at 22°C except for one set made on TPX sheet at 37°C. Two measurement methods were used in the case of TPX films. The apparatus used in both methods is depicted in Figure 1. One method (method 1)

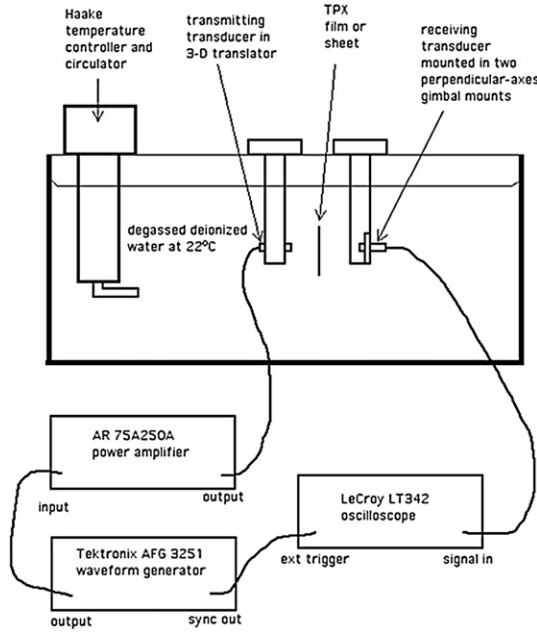


Fig. 1. Diagram of apparatus used for speed and attenuation coefficient measurements. For the through-transmission/water displacement method, reverberations within the sample were avoided by measuring the amplitude and arrival time shift using the first few cycles of the waveform, whereas for the water – TPX – water transmission coefficient method, all significant contributing reverberations were accounted for by using the cycles late in a sufficiently long waveform that amplitudes ceased to vary with time. The distance between transmitting and receiving transducers was 6–10 cm.

was the ordinary through-transmission/water-displacement method (Wear *et al.* 2005). A film with nominal thickness of 268 μm was used. No thicker film is available from the manufacturer. Ten-cycle sinusoidal bursts with frequencies 20 to 72 MHz—in 1-MHz steps—were used for a constant amplitude read-out at each discrete frequency. For frequencies between 20 and 40 MHz, only the first four cycles of the received waveform were addressed because of possible interference later in the waveform caused by reverberations within the film. The sinusoidal bursts generated by the Tektronix AFG 3251 waveform generator were amplified by the Atlantic Research 75A250A power amplifier and output to the transmitting transducer. For frequencies between 20 and 40 MHz, a matched pair of single-element, unfocused, 6-mm-diameter, nominal 30-MHz transducers – with a bandwidth of 80% at –6-dB – were used, one as the transmitter and one as the receiver (V356, Olympus-Panametrics, Waltham, MA, USA). For frequencies between 40 and 72 MHz, a matched pair of single-element, unfocused, 6-mm-diameter, nominal 50-MHz transducers – with a bandwidth of 78% at –6-dB – were used (V358, Olympus-Panametrics). The peak-to-peak excitation voltages were set as low as possible while assuring that signal-to-noise ratios (SNRs)

were not a source of error. Typically, the excitation voltages were about 100 mV, but at 70 MHz, values as high as 1 V were needed. Because of the high frequencies, it was very important to make sure that the received beam was centered on the receiving element. As shown in Figure 1, one transducer was mounted on a 3-D translator and the other on a gimbal mount with vertical and horizontal axes of rotation. These translators and rotators allowed peaking of the received signal at each frequency in the absence of the sample (water path only). For each frequency, two signals were monitored: one with the TPX sample absent and one with the sample interposed between the transmitter and receiver. The amplitudes were recorded for each frequency and the arrival time shift (which depends on the sample thickness) at every 5-MHz interval. It was advantageous to use the random interleave property of the oscilloscope for optimal determinations of the amplitude ratios and time shifts. The distance between the transmitting and receiving elements was between 6 cm and 10 cm, the distance generally decreasing with increasing frequency to allow sufficient SNRs. (At higher frequencies, water attenuation becomes considerable.) As a result, it was not possible for the receiver to be in the far field at all frequencies. Varying the axial position of the sample had no effect on the received signal, however; thus, beam distortions caused by the presence of the sample were considered negligible. The propagation speed is given by (Kremkau *et al.* 1981):

$$c_{TPX} = \frac{c_w}{1 + (c_w \Delta t)/d}, \quad (1)$$

where $c_w = 1488.3$ m/s is the propagation speed in pure water at 22°C (Del Grosso and Mader 1972), d is the thickness of the TPX sample and Δt is the time shift when the sample is inserted. When $\Delta t < 0$, $c > c_w$. The attenuation coefficient in dB per unit length is given by

$$\alpha_{TPX} = \frac{20}{d} \log_{10} \left(\frac{A_0 T_{tot}}{A} \right) + \alpha_w, \quad (2)$$

where A_0 is the amplitude in the absence of the sample, A is that when the sample is interposed, T_{tot} is the amplitude transmission coefficient caused by both surfaces of the sample and α_w is the attenuation coefficient in dB per unit length of pure water at 22°C (Kaye and Laby 1973).

$T_{tot} = \frac{4r_w r_{TPX}}{(r_w + r_{TPX})^2}$ (see Appendix for derivation), where r_w is the acoustic impedance of water and r_{TPX} is the acoustic impedance of the sample. The sample density, taken from manufacturer's tabulated data, is 0.833 g/mL.

The other method (method 2) for determining TPX film attenuation coefficients used the technique described previously for the case of Saran Wrap film (Wear *et al.* 2005). In that technique, the modulus of

the (water – TPX film – water) transmission coefficient is first determined where all reverberations occurring within the TPX film that are not negligible *contribute* to the monitored part of the received signal. (In method 1, all reverberations are avoided.) Monitoring the peak-to-peak amplitude using the last 10 cycles of a 40-cycle tone burst will adequately account for all reverberations for the frequencies considered in this work.

That monitoring the peak-to-peak amplitude using the last 10 cycles of a 40 cycle tone burst will adequately account for all possible contributing reverberations can be shown as follows. Each successive reverberation contributes (*via* interference) no more than $R^2 e^{-2d\alpha}$ times the last reverberation where R is the amplitude reflection coefficient at a planar interface between water and TPX (Kinsler et al. 1982), d is the TPX thickness (128 μm) and α = TPX attenuation coefficient at the frequency involved. Considering the TPX propagation speed to be 2090 m/s and its density 0.833 g/mL and the propagation speed in water to be 1488 m/s and density 1 g/mL, $R^2 = 0.00614$, the first reverberation will thus have an amplitude of <0.00614 times that of the transmitted wave with no reverberation, and the next reverberation will have an amplitude of less than $(0.00614)^2 = 3.8 \times 10^{-5}$ times that of the transmitted wave with no reverberation, *etc.* (The attenuation factor, which is always less than 1, is ignored.) Thus, only the first reverberation makes a measurable contribution. The wavelength in TPX at frequency f is $\lambda = 2090 \mu\text{m} \mu\text{s}^{-1}/f$, and the number of wavelengths in $2d = 256 \mu\text{m} / \lambda$. For 20–72 MHz, the greatest number of wavelengths in 2-D is <9 . Thus, measurement of the peak-to-peak amplitude in the last 10 cycles of a 40-cycle tone burst will ensure that all reverberations are adequately accounted for.

At each frequency, the received amplitudes with and without the TPX film present were determined. The mount for the TPX film is shown in Figure 2, where water existed both inside and outside of the cylinder and the polyethylene film window was absent, to ensure equal water pressures on each side of the TPX film. The TPX film was mounted flat on a square acrylic frame that was screwed onto the acrylic cylinder. Data reduction was accomplished using eqn (1) from Wear et al. (2005), *viz*,

$$T = \frac{2r_w}{2r_w \cos(k_{TPX}d) + j \left(r_{TPX} + \frac{r_w^2}{r_{TPX}} \right) \sin(k_{TPX}d)}, \quad (3)$$

where $j = \sqrt{-1}$; r_w , r_{TPX} and d are defined in the last paragraph; and $k_{TPX} = \frac{2\pi f}{c_{TPX}} - j\alpha_{TPX}$. The derivation of eqn (3) is available in Ford (1971). The modulus, $|T|$,

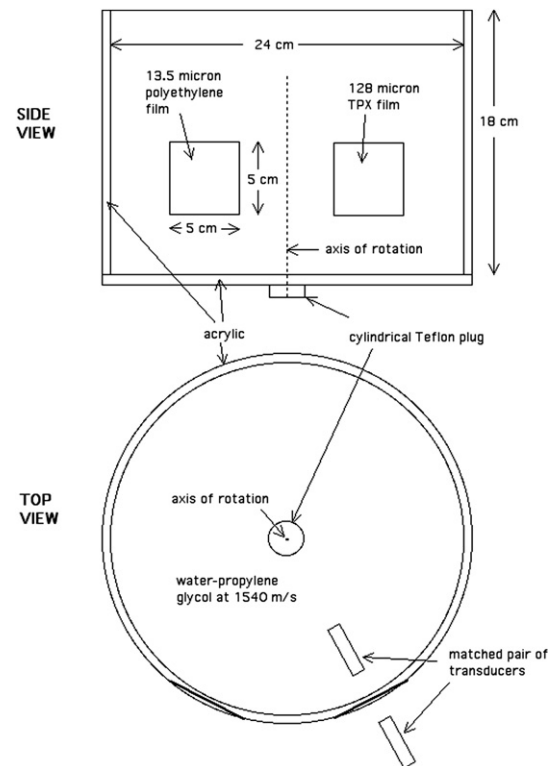


Fig. 2. Diagram of liquid barrier apparatus used in measurement of the round-trip “Total” transmission coefficient: water – TPX film – 1540 m/s liquid – TPX film – water. The cylinder is fixed in position in the water tank of Fig. 1 and can be rotated about the vertical axis of rotation so that the ultrasound beam from the transmitter to receiver can be aligned perpendicular to either the polyethylene window or the TPX film. Degassed, deionized tank water surrounds the cylinder, and a solution of propylene glycol and water with a propagation speed of 1540 m/s exists inside the cylinder. Note that the same apparatus was used in method 2 with water inside and outside the cylinder.

was measured at each frequency f and then α_{TPX} was determined over the frequency range by least-squares fitting to $|T|$ values using a power law representation of α_{TPX} , *i.e.*, $\alpha_{TPX} = B f^n$, where B and n are constants. The TPX propagation speed c_{TPX} used in the data reduction was that determined from method 1. TPX film having a nominal thickness of 128 μm was used. Note that the 268- μm -thick film was used in method 1 to avoid reverberation within the film at all frequencies involved, whereas there was no such restriction for method 2, and the 128- μm film was used in method 2 to optimize received signal-to-noise ratios. Six thickness measurements were made around the area through which the beam passed, resulting in a mean and sample standard deviation of $127.8 \pm 2.9 \mu\text{m}$; a National Institute of Standards and Technology (NIST) traceable calibrated micrometer was used (Code number 293-340, Mitutoyo America Corp., Elk Grove Village, IL). The measurement

uncertainty for a single measurement at 20°C is $\pm 1.3 \mu\text{m}$ for this thickness; thus, by propagation of uncorrelated errors, the total uncertainty is $\pm 3.2 \mu\text{m}$. The propagation of uncorrelated errors was used as applied to calibration (systematic) and random errors (Taylor 1997).

Test of the capacity to predict transmission coefficients

Data acquisition. An assessment of the uncertainty estimates for TPX film propagation speeds and attenuation coefficients was carried out by comparing directly measured transmission coefficients for TPX film between two different media with transmission coefficients computed using the measured values of TPX propagation speeds and attenuation coefficients. The two media chosen were water and a solution of propylene glycol and water having a tissue-like propagation speed of 1540 m/s. These two media are relevant to some preclinical laboratory measurements where the reference phantom method is used to estimate the attenuation and backscatter coefficients of tumors hosted by small animals, and a water path exists between the tumor and the transducer. The choice of media is also relevant to clinical skin tissue characterization in which it may be desirable to include a variable water path stand-off so that the focus of a single-element transducer can be positioned at various depths. Application of the reference phantom method in these preclinical and clinical examples would involve production of a matching water path length between the transducer and TPX film.

The apparatus used has been described previously (Stiles *et al.* 2008). It consists of the same apparatus as in Figure 1, except that a cylindrical acrylic liquid barrier with vertical TPX and polyethylene windows exists in the water tank of Figure 1. The barrier is diagrammed in Figure 2.

Ideally, there would be direct contact between the water and propylene glycol/water solution, but that is impossible because the two would mix. Although the polyethylene (PE) window is thin ($13.5 \mu\text{m}$ = about 2 wavelengths at 70 MHz), its presence nevertheless must be accounted for in the data reduction to determine the modulus of the TPX film total transmission coefficient. The modulus of the PE total transmission coefficient is much closer to 1 than in the case of TPX (see Figs. 11 and 12), so the correction is small ($\leq 13\%$) but must be included. The matched pair of transducers is first aligned so that their symmetry axes are approximately colinear and perpendicular to the polyethylene film. Then with 40-cycle sinusoidal US bursts being generated, the amplitude of the received signal is maximized. (Forty cycles were sufficient that the last part of the received waveform had constant amplitude over all frequencies involved.) The cylinder is then rotated by a small amount

to further maximize the received signal; the later step assures that the film is perpendicular to the US beam. The peak-to-peak voltage amplitude is recorded and the cylinder rotated so that the beam passes through the TPX film; the received amplitude is again maximized, and the peak-to-peak voltage amplitude is recorded. Then the transmitter/receiver roles of the transducers are switched, peaking of the received signals again done and peak-to-peak voltage amplitudes recorded with polyethylene and then TPX in position. Seven matched pairs of broadband unfocused transducers were used to span the range of frequencies from 0–70 MHz; the nominal frequencies were 2.5, 5, 7, 10, 15, 30 and 50 MHz. Data were obtained in 2-MHz steps.

Data analysis: accounting for the transmission coefficient of the polyethylene film. Two relations (eqns (10) and (13), listed later) are derived to account for the transmission coefficients of the polyethylene film. The subscript 1 refers to water and the subscript 2 refers to the propylene glycol/water solution. Table 1 lists the definitions of the parameters involved in the derivation.

We have moduli of

$$\|T_{1 \rightarrow 2}^{TPX}\| = \frac{A_2^{TPX}}{A_1} \quad \text{and} \quad \|T_{1 \rightarrow 2}^{PE}\| = \frac{A_2^{PE}}{A_1}. \quad (4)$$

Assume that the TPX and PE films are sufficiently thin that the diffraction pattern at the receiver is the same for TPX and PE. (This assumption was justified experimentally when no change in received amplitude occurred when the TPX film was moved from being within 1 cm of the transmitter to within 1 cm of the receiver—including 70 MHz.)

Then

$$\frac{V_2^{TPX}}{A_2^{TPX}} = \frac{V_2^{PE}}{A_2^{PE}}. \quad (5)$$

From eqn (4):

$$\frac{1}{A_1} = \frac{\|T_{1 \rightarrow 2}^{PE}\|}{A_2^{PE}} \quad \text{and} \quad \|T_{1 \rightarrow 2}^{TPX}\| = \|T_{1 \rightarrow 2}^{PE}\| \left(\frac{A_2^{TPX}}{A_2^{PE}} \right). \quad (6)$$

From eqn (5):

$$\|T_{1 \rightarrow 2}^{TPX}\| = \|T_{1 \rightarrow 2}^{PE}\| \left(\frac{V_2^{TPX}}{V_2^{PE}} \right). \quad (7)$$

Exchanging 1 and 2 in all of the above, we have

$$\|T_{2 \rightarrow 1}^{TPX}\| = \|T_{2 \rightarrow 1}^{PE}\| \left(\frac{V_1^{TPX}}{V_1^{PE}} \right). \quad (8)$$

Then the modulus of the total transmission coefficient for TPX in terms of that for polyethylene is

Table 1. Definitions of parameters involved in the derivation of eqns (10) and (13)

$T_{1 \rightarrow 2}^{TPX}$	Amplitude transmission coefficient through TPX from medium 1 to medium 2
$T_{2 \rightarrow 1}^{TPX}$	Amplitude transmission coefficient through TPX from medium 2 to medium 1
$T_{1 \rightarrow 2}^{PE}$	Amplitude transmission coefficient through polyethylene (PE) from medium 1 to medium 2
$T_{2 \rightarrow 1}^{PE}$	Amplitude transmission coefficient through PE from medium 2 to medium 1
T_{tot}^{PE}	Product of $T_{2 \rightarrow 1}^{PE}$ and $T_{1 \rightarrow 2}^{PE}$
A_n	Pressure amplitude of wave incident on TPX or PE from medium n (n = 1 or 2)
A_n^{TPX}	Pressure amplitude of wave passing from TPX into medium n (n = 1 or 2)
A_n^{PE}	Pressure amplitude of wave passing from PE into medium n (n = 1 or 2)
V_n^{TPX}	Peak-to-peak voltage amplitude of received signal in medium n when TPX is in place (n = 1 or 2)
V_n^{PE}	Peak-to-peak voltage amplitude of received signal in medium n when PE is in place (n = 1 or 2)

The subscript 1 refers to water and the subscript 2 refers to the propylene glycol/water solution.

$$\|T_{tot}^{TPX}\| = \|T_{1 \rightarrow 2}^{TPX}\| \times \|T_{2 \rightarrow 1}^{TPX}\| = \|T_{1 \rightarrow 2}^{PE}\| \times \|T_{2 \rightarrow 1}^{PE}\| \times \left(\frac{V_2^{TPX}}{V_2^{PE}}\right) \left(\frac{V_1^{TPX}}{V_1^{PE}}\right) = \|T_{tot}^{PE}\| \left(\frac{V_2^{TPX}}{V_2^{PE}}\right) \left(\frac{V_1^{TPX}}{V_1^{PE}}\right); \quad (9)$$

thus, we have

$$\|T_{tot}^{TPX}\| = \|T_{tot}^{PE}\| \left(\frac{V_2^{TPX}}{V_2^{PE}}\right) \left(\frac{V_1^{TPX}}{V_1^{PE}}\right). \quad (10)$$

The amplitude transmission coefficients $T_{1 \rightarrow 2}^{PE}$ and $T_{2 \rightarrow 1}^{PE}$ are computed using eqn (1) in Wear et al. (2005) as follows:

$$T_{1 \rightarrow 2}^{PE} = \frac{2r_{PG/w}}{(r_w + r_{PG/w})\cos(k_{PE}d_{PE}) + j\left(r_{PE} + r_w r_{PG/w}/r_{PE}\right)\sin(k_{PE}d_{PE})} \quad (11)$$

and

$$T_{2 \rightarrow 1}^{PE} = \frac{2r_w}{(r_w + r_{PG/w})\cos(k_{PE}d_{PE}) + j\left(r_{PE} + r_w r_{PG/w}/r_{PE}\right)\sin(k_{PE}d_{PE})}. \quad (12)$$

where r_w is the acoustic impedance of water, $r_{PG/w}$ is the acoustic impedance of the propylene glycol/water solution, r_{PE} is the acoustic impedance of polyethylene, and d_{PE} is the thickness of the PE film. The complex wave number value is $k_{PE} = 2\pi f/c_{PE} + j\alpha_{PE}$, where c_{PE} = the polyethylene propagation speed and α_{PE} = the polyethylene attenuation coefficient at the frequency of concern. The value for c_{PE} was taken from tables in Kaye and Laby (1973), and the values for α_{PE} were determined experimentally. (See relevant subsection in the Results section.)

Thus, from eqns (11) and (12),

$$\|T_{tot}^{PE}\| = \frac{4r_w r_{PG/w}}{\|(r_w + r_{PG/w})\cos(k_{PE}d) + j\left(r_{PE} + r_w r_{PG/w}/r_{PE}\right)\sin(k_{PE}d)\|^2}. \quad (13)$$

The mass density of the polyethylene film was measured by submerging an approximately 0.5-cm² piece of the polyethylene film in a solution of 1-bromododecane (density, 1.038 g/mL) and tetradecane (density, 0.763 g/mL) (Sigma Chemical, St. Louis, MO, USA). The solution was computed to have a density of ~0.91 g/mL. Addition of small amounts of 1-bromododecane and/or tetradecane, while stirring to make uniform solutions, resulted in the polyethylene film neither rising nor sinking. The density of the final solution (and of the polyethylene film) was then measured with a calibrated hydrometer (Catalog number 11-556D, Fisher Scientific, Pittsburgh, PA, USA) with the result of 0.919 g/mL.

Voltages applied to the transmitting transducers

It may be of interest to researchers who would like to use the measurement methods described here to know the peak-to-peak voltages applied to the transmitting transducers. For all measurements described here, a six-foot RG 58 immersion coaxial cable connected the output of the power amplifier to the transducer. Because the wavelength of the transmitted voltage at 70 MHz is about 3 meters, the six-foot cable length could result in different peak-to-peak voltages at each end of the cable. Therefore, we measured the voltages using a substitute six-foot

RG 58 cable with a T having a UHF connector for the transducer and a BNC connector for the oscilloscope input; the input impedance of the scope was 1 M Ω . (At 70 MHz, the peak-to-peak voltage at the transducer was about 90% of that at the power amplifier output.) Also, all peak-to-peak voltages were measured with the emitting end of the transducer immersed in water. Tables 2 and 3 show these voltages for each measurement event.

RESULTS

All results correspond to measurements at 22°C except for a set of measurements at 37°C for TPX sheet.

Speed and attenuation coefficients of the TPX film

Method 1. Figure 3 shows attenuation coefficients from 20–70 MHz measured at 1-MHz intervals using method 1 on a nominal 268- μ m-thick sample of TPX film. The curve resulting from a least-squares-fit to a power law is shown in the figure. That power law result is

$$\alpha_{\text{TPX}}^{\text{meth1}} = 1.038 f^{1.284} \text{ dB cm}^{-1} \text{ MHz}^{-1.284}. \quad (14)$$

For reference, the value of $\alpha_{\text{TPX}}^{\text{meth1}}$ at 40 MHz is 118.4 dB cm⁻¹.

Table 2. Transducer models and peak-to-peak voltages applied to transmitting transducers for measurements at 2-MHz intervals (where applicable)

Frequency (MHz)	Method 1: TPX film		Method 2: PE film		Transmission: H ₂ O → TPX → propylene glycol solution		Transmission: propylene glycol solution → TPX → H ₂ O	
	p-p volts	Transmitter model	p-p volts	Transmitter model	p-p volts	Transmitter model	p-p volts	Transmitter model
2	—	—	—	—	0.857	V306*	0.857	V306*
4	—	—	—	—	0.766	V309†	0.766	V309†
6	—	—	—	—	0.552	V309†	0.552	V309†
8	—	—	—	—	0.656	V320‡	0.656	V320‡
10	—	—	—	—	0.369	V311§	0.369	V311§
12	—	—	—	—	0.49	A319S¶	0.49	A319S¶
14	—	—	—	—	0.54	A319S¶	0.54	A319S¶
16	—	—	—	—	0.517	A319S¶	0.353	A319S¶
18	—	—	—	—	0.545	A319S¶	0.442	A319S¶
20	29.6	V358	8.34	V358	2.35	V356	0.451	A319S¶
22	29.6	V358	8.52	V358	2.42	V356	8.52	V356
24	31.2	V358	8.93	V358	2.51	V356	8.93	V356
26	34.3	V358	9.85	V358	2.66	V356	9.85	V356
28	39.1	V358	11.26	V358	2.79	V356	11.26	V356
30	47.0	V358	13.22	V358	2.87	V356	13.22	V356
32	56.5	V358	16.4	V358	3.05	V356	16.4	V356
34	65.9	V358	19.1	V358	19.1	V358	19.1	V358
36	69.7	V358	20.3	V358	20.3	V358	20.3	V358
38	65.9	V358	19.0	V358	19.3	V358	19.0	V358
40	56.8	V358	16.4	V358	17.5	V358	16.4	V358
42	52.6	V358	22.6	V358	22.6	V358	10.62	V358
44	50.1	V358	21.4	V358	23.7	V358	9.62	V358
46	49.7	V358	28.3	V358	21.2	V358	8.62	V358
48	50.1	V358	28.5	V358	19.1	V358	7.22	V358
50	50.6	V358	57.9	V358	17.1	V358	50.6	V358
52	50.6	V358	57.4	V358	50.6	V358	50.6	V358
54	68.8	V358	55.4	V358	55.4	V358	21.0	V358
56	65.2	V358	52.4	V358	14.63	V358	26.2	V358
58	60.9	V358	49.2	V358	60.9	V358	55.1	V358
60	56.8	V358	45.6	V358	56.8	V358	51.2	V358
62	52.9	V358	88.9	V358	25.4	V358	40.3	V358
64	49.9	V358	84.5	V358	43.5	V358	43.5	V358
66	69.1	V358	47.2	V358	69.1	V358	69.1	V358
68	64.7	V358	44.2	V358	53.6	V358	64.7	V358
70	60.2	V358	73.8	V358	73.8	V358	60.2	V358
72	—	—	69.3	V358	—	—	—	—

For all frequencies of 20–72 MHz, the transmitting and receiving transducers are Panametrics (Olympus) matched pairs. For 2–18 MHz the transmitter is Panametrics, but the receiver is different (Panametrics or AeroTech); makes and models are listed below.

* Aerotech Delta PN2794-1.

† Aerotech Delta PN2794-3.

‡ Aerotech Delta PN2794-4.

§ Delta OOJWM4.

¶ Panametrics A313S.

Table 3. Transducer models and peak-to-peak voltages applied to transmitting transducers for measurements at 2.5- or 5-MHz intervals

Frequency (MHz)	Method 2: TPX film		Method 1: TPX sheet	
	p-p volts	Transmitter model	p-p volts	Transmitter model
10	—	—	2.02	V311*
15	—	—	0.679	A319S†
20	8.34	V358	8.48	V358
22.5	6.56	V358	—	—
25	7.11	V358	9.39	V358
27.5	8.16	V358	—	—
30	9.98	V358	13.36	V358
32.5	12.9	V358	—	—
35	19.9	V358	20.30	V358
37.5	19.5	V358	—	—
40	16.4	V358	36.60	V358
42.5	22.3	V358	—	—
45	21.3	V358	32.30	V358
47.5	28.5	V358	—	—
50	28.7	V358	32.70	V358
52.5	36.5	V358	—	—
55	40.8	V358	10.35	V358
57.5	49.9	V358	—	—
60	56.8	V358	11.58	V358
62.5	52.2	V358	—	—
65	66.6	V358	14.59	V358
67.5	76.4	V358	—	—
70	73.8	V358	20.40	V358
72.5	75.2	V358	—	—

For all frequencies of 20–72.5 MHz, the transmitting and receiving transducers are Panametrics (Olympus) matched pairs. For 10 and 15 MHz, the transmitter and receiver are Panametrics, but the receiver model is different as noted below.

* Delta OJWM4.

† Panametrics A313S.

Figure 4 shows measured propagation speeds at 5-MHz intervals with a least-squares-fitted Kramers-Kronig curve computed using the approximation in eqn (3b) in O'Donnell et al. (1981), *viz.*,

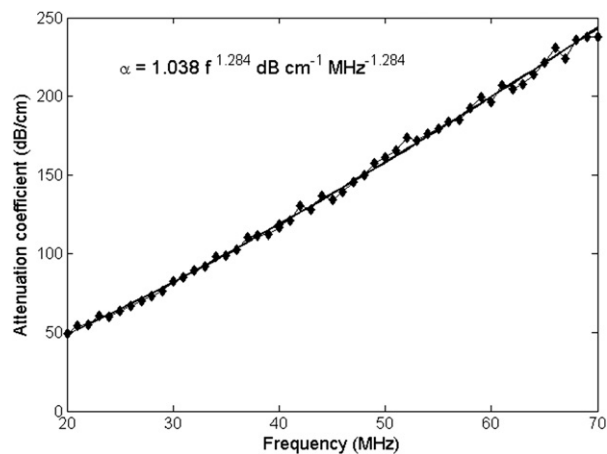


Fig. 3. Attenuation coefficients of TPX film measured using method 1 (◆) and the resulting power law fit (solid line). The power law fit is given in eqn (14).

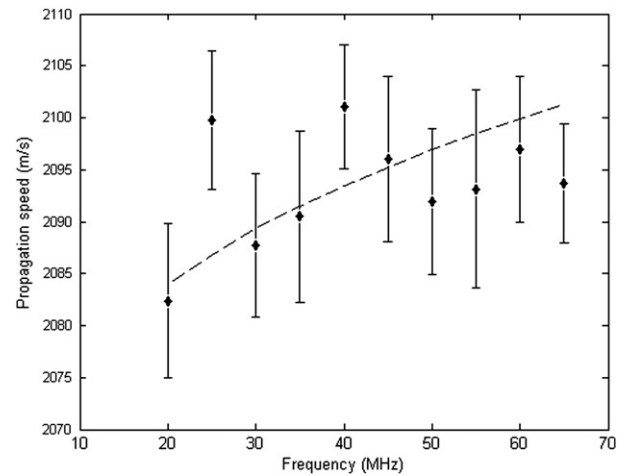


Fig. 4. Propagation speeds of TPX film measured using method 1 (◆). The error bars account for precision and sample thickness uncertainties. The dashed curve is the Kramers-Kronig prediction where least-squares-fitting using eqn (15) determined the position of the curve.

$$c(\omega) = c(\omega_0) + \frac{2c^2(\omega_0)}{\pi} \int_{\omega_0}^{\omega} \frac{\alpha(\omega')}{\omega'^2} d\omega', \quad (15)$$

where $c(\omega_0)$ is the speed at some angular frequency ω_0 and ω is any angular frequency in the range over which the attenuation coefficient α has been measured; $c(\omega_0)$ is varied to accomplish the least-squares fitting. The error in propagation speeds strongly depends on the sample thickness uncertainty. Thickness measurements at eight positions in the area of the sample where the beam passed through resulted in a mean and sample standard deviation of $269.5 \pm 1.6 \mu\text{m}$.

Method 2. Figure 5 shows measured values of the water – TPX film – water transmission coefficient moduli, $|T_{w \rightarrow w}^{\text{TPX}}|$, from 20–72.5 MHz in 2.5-MHz increments. The solid curve corresponds to the best fit to the experimental values assuming a power law for TPX film attenuation coefficients and a mean propagation speed of 2093 m/s (see Fig. 4). Note that, even though the first reverberation has a very small amplitude, its effect is demonstrated in Figure 5 from 20 through ~50 MHz. The resulting power law for TPX film attenuation coefficients is

$$\alpha_{\text{TPX}}^{\text{meth2}} = 0.906 f^{1.324} \text{ dB cm}^{-1} \text{ MHz}^{-1.324}. \quad (16)$$

At 40 MHz $\alpha_{\text{TPX}}^{\text{meth2}} = 119.7 \text{ dB cm}^{-1}$, which is within 1.1% of the value obtained using method 1.

A comparison of the attenuation coefficients for TPX film using methods 1 and 2 is shown in Figure 6. The dotted line corresponds to method 1 (eqn (14)) and the dashed line to method 2 (eqn (16)).

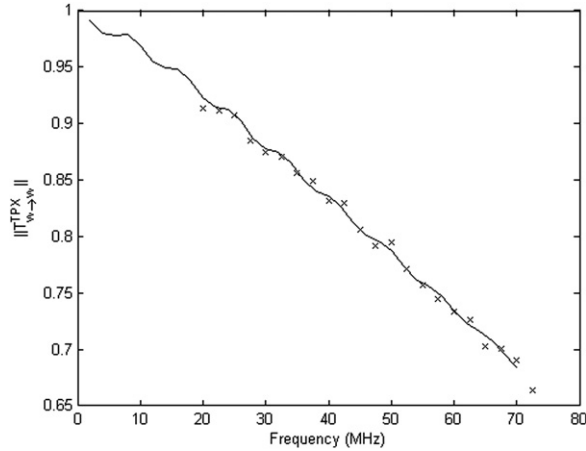


Fig. 5. Measured values of the moduli of the water – TPX film – water transmission coefficient from 20–72.5 MHz (x) and the transmission coefficient moduli computed using the mean propagation speed from Fig. 4 and the power law for the attenuation coefficients (*solid line*), corresponding to eqn (16), which yields optimal agreement with the measured values. Optimal agreement was determined by iterating the values of α_0 and n in the assumed attenuation coefficient relation $\alpha = \alpha_0 f^n$, where f is the frequency and α_0 and n are constants, until the computed transmission coefficient passed through the middle of the distribution of experimental points over the 20–70-MHz range.

Speed and attenuation coefficients of TPX sheet

Measurements of the attenuation coefficients and propagation speeds on TPX sheet were done using only method 1 because production of sufficiently thin sheets was not practical for application of method 2 because of the high attenuation. Figure 7 shows measured values of attenuation coefficients from 10 through 70 MHz

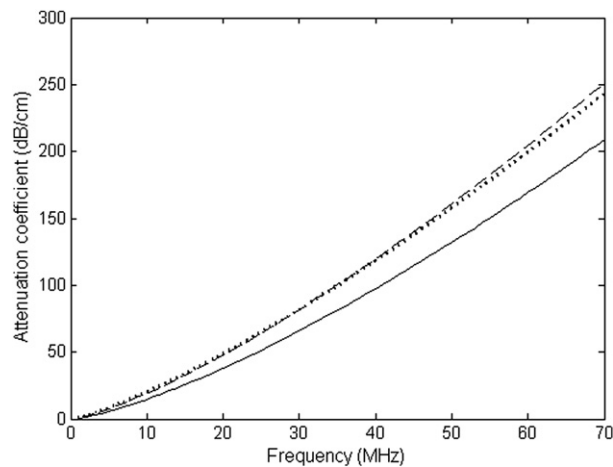


Fig. 6. Comparison of TPX film attenuation coefficients determined using method 1 (*dotted line*) and method 2 (*dashed line*). Also shown are the attenuation coefficients for TPX sheet (*solid line*) showing the considerable difference between the film and sheet values, *i.e.*, at 50 MHz, the TPX sheet value is 83% of the mean value for the TPX film.

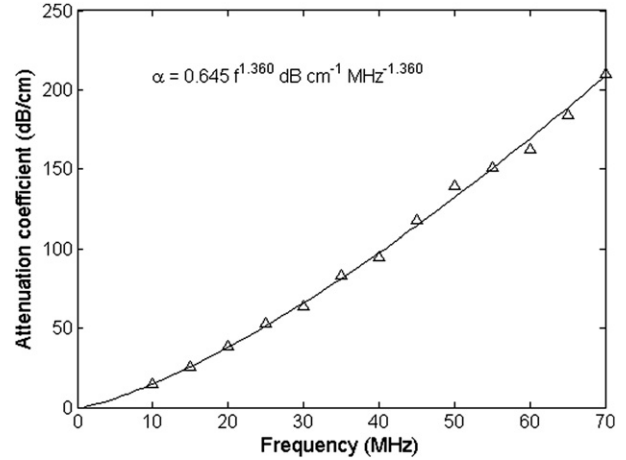


Fig. 7. Experimental values of attenuation coefficients for TPX sheet (Δ) and least-squares curve-fit to the data (*solid line*). The solid line corresponds to a least-squares curve-fit to the experimental points (eqn (17)).

at 5-MHz intervals. The solid curve results from least-squares-curve fitting to a power law, which is

$$\alpha_{\text{TPX}}^{\text{meth1}} = 0.645 f^{1.360} \text{ dB cm}^{-1} \text{ MHz}^{-1.360}. \quad (17)$$

For comparison with the 118.4 dB cm^{-1} value for TPX film at 40 MHz, the value for TPX sheet is 97.4 dB cm^{-1} at 40 MHz, *i.e.*, the sheet value is about 18% less than the film value.

Figure 8 shows measured propagation speeds at 5-MHz intervals with a least-squares-fitted Kramers-Kronig relation (eqn (15)). Two thicknesses (2.39 mm and 1.47 mm) were used, one corresponding to the filled diamonds and the other to the open diamonds. The

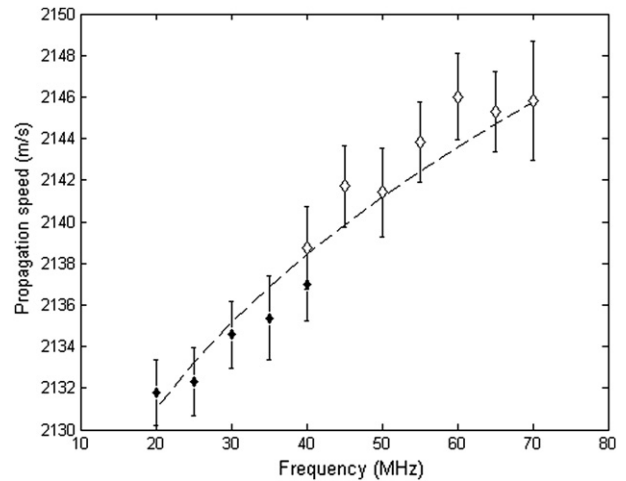


Fig. 8. Experimental values of propagation speed for 20–40 MHz (◆) correspond to a mean sample thickness and standard deviation of $2.3916 \pm 0.0041 \text{ mm}$, and values for 40–70 MHz (◇) correspond to a mean sample thickness and standard deviation of $1.4692 \pm 0.0030 \text{ mm}$. Error bars account for precision and uncertainty in sample thickness. The dashed curve results from least-squares-fit of eqn (15).

thickness error propagated into the speed values is the same for all filled diamonds and for all open diamonds, *i.e.*, there are two thickness error values—one for the filled diamonds and another for the open diamonds.

Because TPX sheet could be used in a transducer in contact with a patient's skin, attenuation coefficients and propagation speeds were measured at 37°C. Regarding temperature dependencies of TPX sheet, it was found that the attenuation coefficients of TPX sheet increase by about 8%, and the propagation speed decreases by about 65 m/s (3%) as the temperature rises from 22–37°C (body temperature). Attenuation coefficient results at 37°C are shown in Figure 9 (compare with values in Figure 7). The propagation speed was measured at 40 MHz and was 2073 m/s.

Speed and attenuation coefficients of polyethylene film

Only method 2 was used to estimate attenuation coefficients of the polyethylene film because thicker samples than the 13.5- μm form were not available from the manufacturer, and 13.5 μm is too thin to facilitate use of method 1. The propagation speed of 2000 m/s was taken from tables in Kaye and Laby (1973).

Figure 10 shows data points for the transmission coefficient moduli measured at 2-MHz intervals from 2–72 MHz. The solid curve is a graph of the best obtainable fit to the data assuming a power law for the attenuation coefficients. The fit was derived by inserting the speed and trial power law relations for the attenuation coefficients into eqn (3), where the subscript TPX is replaced with PE (polyethylene). The resulting relation for the attenuation coefficients of the polyethylene film is

$$\alpha_{\text{PE}}^{\text{meth2}} = 8.88 f^{0.92} \text{ dB cm}^{-1} \text{ MHz}^{-0.92}, \quad (18)$$

and the result of the fit is shown in Figure 10. For reference, the value of $\alpha_{\text{PE}}^{\text{meth2}}$ at 40 MHz is 264.4 dB cm^{-1} .

Prediction of round-trip transmission coefficients between different media

Figures 11 and 12 show comparisons of experimentally determined (Δ) values of $\|T_{\text{tot}}^{\text{TPX}}\|$ and predicted—or computed—values (*solid lines*) of $\|T_{\text{tot}}^{\text{TPX}}\|$ from 2–70 MHz; Figures 11 and 12 differ regarding whether method 1 or 2 was used to determine the propagation speeds and attenuation coefficients that were used in the computation of $\|T_{\text{tot}}^{\text{TPX}}\|$. The computed values of $\|T_{\text{tot}}^{\text{TPX}}\|$ were found using the relation

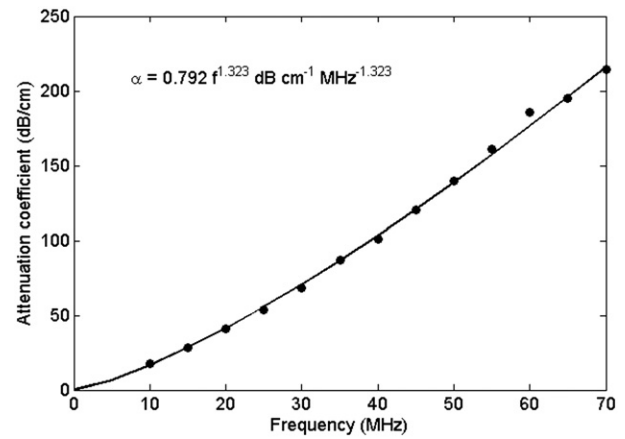


Fig. 9. Attenuation coefficients of the TPX sheet at 37°C. The solid line corresponds to a least-squares-fit to the experimental points; the curve-fit equation is also shown in the figure.

where r_{TPX} is the acoustic impedance of the TPX film and $k_{\text{TPX}} = \frac{2\pi f}{c_{\text{TPX}}} - j\alpha_{\text{TPX}}$ is the complex wave number. Equation (19) corresponds to eqn (13), where PE is replaced with TPX. The dashed lines in Figures 11 and 12 correspond to application of eqn (13) and are used in the determination of the experimental values $\|T_{\text{tot}}^{\text{TPX}}\|$ as described in “Data analysis: accounting for the transmission coefficient of the polyethylene film.”

Summary

Attenuation coefficients and propagation speeds for TPX film were measured using method 1. Propagation speeds are shown in Figure 4. The errors are dominated by the thickness uncertainty. Conformity to the Kramers-Kronig relations is one test of the accuracy of measurements of these two parameters. Using the Kramers-Kronig relation in eqn (15) with attenuation coefficients in eqn (14), a least-squares fit to the measured speed values resulted in the prediction given by the dashed line in Figure 4. Although conformity of the measured values to the Kramers-Kronig prediction is not confirmed, it is also not contradicted.

Method 2 was also used to measure the attenuation coefficients of the TPX film from 20–72.5 MHz. Using the mean speed found with method 1 and trial power law representations for the attenuation coefficients in eqn (3) resulted in the excellent fit to the data seen in Figure 5. The resulting optimal power law for the attenuation coefficients is given by eqn (16). In Figure 6

$$\|T_{\text{tot}}^{\text{TPX}}\| = \frac{4r_w r_{\text{PG}/w}}{\left\| (r_w + r_{\text{PG}/w}) \cos(k_{\text{TPX}} d) + j \left(r_{\text{TPX}} + r_w r_{\text{PG}/w} / r_{\text{TPX}} \right) \sin(k_{\text{TPX}} d) \right\|^2}, \quad (19)$$

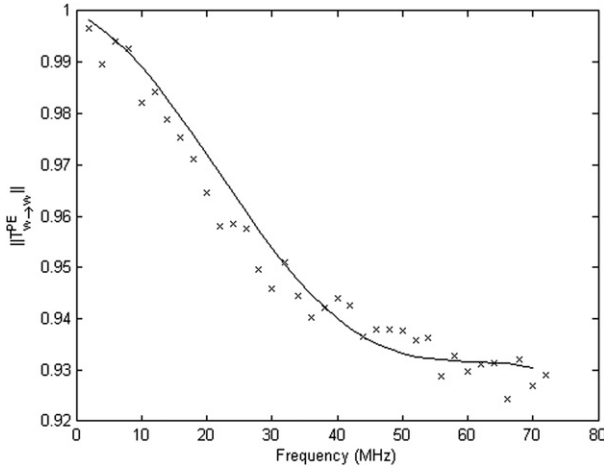


Fig. 10. Measured values of the water – PE film – water transmission coefficient moduli from 2–72 MHz (x) and the transmission coefficient moduli computed using a mean propagation speed of 2000 m/s and a power law for the attenuation coefficients (solid line), corresponding to eqn (18), which yields optimal agreement with the measured values. Optimal agreement was determined by iterating the values of α_0 and n in the assumed attenuation coefficient relation $\alpha = \alpha_0 f^n$, where f is the frequency and α_0 and n are constants, until the computed transmission coefficient moduli were as close as achievable to the middle of the distribution of experimental points over the 20–70-MHz range. Regarding the “leveling off” of the transmission coefficient moduli >40 MHz, there are two competing factors. In the absence of attenuation, there would be a minimum value at 37 MHz (at which the film thickness = $(1/4) \times$ wavelength) with increase at larger frequencies to 1 again at 74 MHz (at which the film thickness = $(1/2) \times$ wavelength); the large attenuation (increasing with frequency) tends to drive the transmission coefficient modulus lower with increasing frequency.

excellent agreement between results using methods 1 and 2 to measure attenuation coefficients is demonstrated; above 40 MHz, the result for method 1 is slightly lower than that for method 2, the greatest difference being about 2%.

Measurements of the attenuation coefficients and propagation speeds on TPX sheet were done using only method 1 because production of sufficiently thin sheets was not practical for application of method 2 because of the high attenuation values obtained in method 1 (see Fig. 7). Least-squares fitting of the attenuation coefficient values yielded eqn (17). The attenuation coefficients of TPX sheet are considerably less than in the case of the TPX film as shown in Figure 6, where the solid line corresponds to eqn (17). For example, at 50 MHz, the TPX sheet value is 83% of the mean value for the TPX film.

Measured values of propagation speeds for TPX sheet are shown in Figure 8 along with the least-squares fitted Kramers-Kronig relation with eqn (17) inserted. Conformity with the Kramers-Kronig prediction is demonstrated.

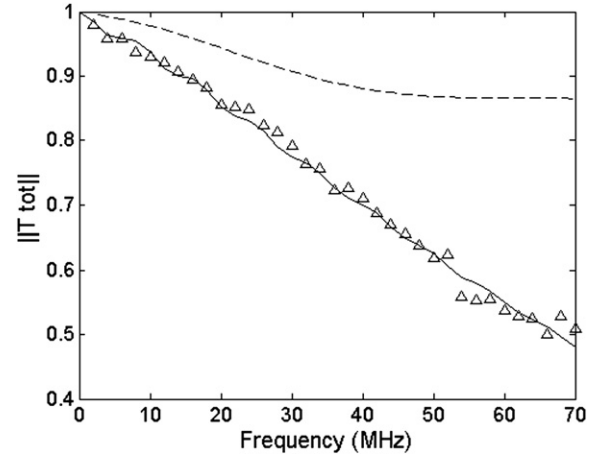


Fig. 11. Experimental values for $\|T^{\text{TPX}}_{\text{tot}}\|$ (Δ) compared with predicted values (solid line). The predicted $\|T^{\text{TPX}}_{\text{tot}}\|$ values were computed with speed and attenuation values determined using method 1; see eqn (14) for attenuation values. The TPX speed value used was the mean of those in Fig. 4. The $\|T^{\text{PE}}_{\text{tot}}\|$ values (dashed line) were computed with a tabulated $c_{\text{PE}} = 2000$ m/s and attenuation values (α_{PE}) determined via method 2 (see eqn (18)).

Only method 2 was practical for measuring the attenuation coefficients of the polyethylene film used in the apparatus described in the subsection “Test of the capacity to predict transmission coefficients.” Because of the very thin material (13.5 μm), it was also not practical to estimate a propagation speed so a value from tables was used. An optimal fit to the water – polyethylene film – water transmission coefficients resulted in eqn (18) for the polyethylene attenuation coefficients.

Figures 11 and 12 demonstrate that the prediction of $\|T^{\text{TPX}}_{\text{tot}}\|$ using attenuation coefficients measured via

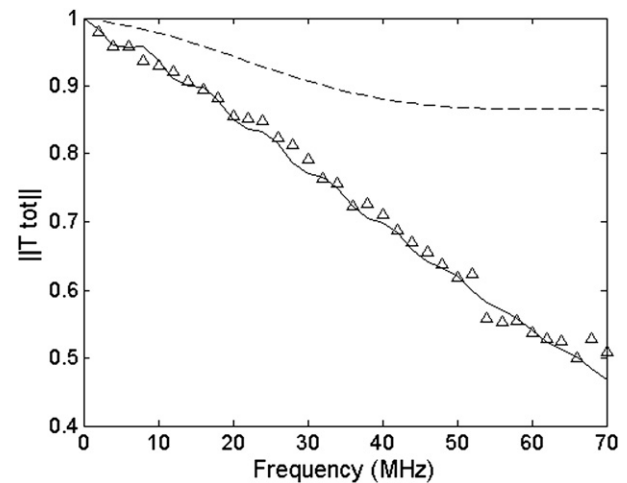


Fig. 12. Same as Figure 11, except that the predicted $\|T^{\text{TPX}}_{\text{tot}}\|$ values (solid line) were determined with attenuation coefficient values using method 2 (see eqn (16)) and the mean speed found using method 1 (see Fig. 4).

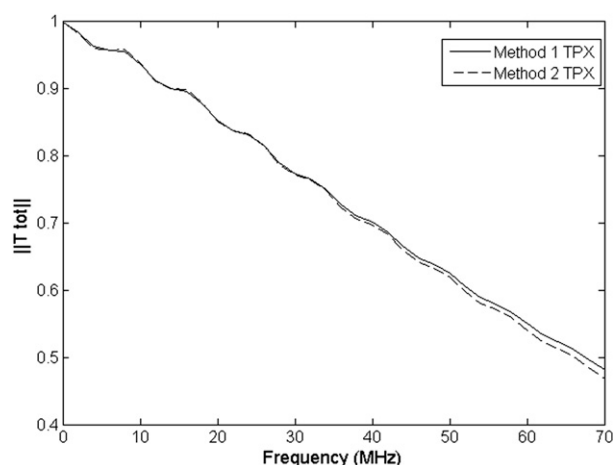


Fig. 13. Comparison of $||T_{\text{tot}}^{\text{TPX}}||$ predicted via from method 1 (solid line) with that predicted via method 2 (dashed line) showing level of agreement between the two.

methods 1 and 2—and speed from method 1—are nearly identical, as expected. A direct comparison is shown in Figure 13. Also, agreement with experimental measurements of $||T_{\text{tot}}^{\text{TPX}}||$ is excellent for both methods. Thus, the validity of using the propagation speed and attenuation coefficients for TPX film to predict transmission coefficients between different media is strengthened.

DISCUSSION

For quantitative ultrasound (QUS), where corrections for the transmission coefficients of the scanning window are needed when the scanning window exists between different media, prediction of the transmission coefficients in the high-frequency range can be made with confidence using the attenuation and speed values reported in this work. However, caution is advised regarding an assumption that the attenuation and speed results presented apply for all TPX film and sheet because it was found that the raw TPX used to manufacture the film or sheet comes in different "grades" and that the process for producing the TPX film is different from that used in the production of TPX sheet. Thus, it is recommended that the results presented in this work be taken to apply only for the particular types of TPX film and sheet investigated.

Clinical implications of this work involve supportive roles. Use of the reference phantom method in the high-frequency range may aid in the diagnosis of diseased tissues through knowledge of *in vivo* attenuation and backscatter coefficients. The success of the reference phantom method will likely require correction for the propagation speed and frequency-dependent attenuation coefficient of a TPX scanning window on the phantom. Knowledge of the high-frequency properties of TPX

may also be valuable regarding the design of future high-frequency scan heads.

Future extensions of this work include characterizing other materials which are—or might be—used by scanner manufacturers in the high-frequency range as acoustic lenses or as coupling layers covering transducer arrays. One type of material is Rexolite (C-LEC Plastics, Philadelphia, PA, USA), which is polystyrene that has been cross-linked in various ways. A form of Rexolite is used on high frequency arrays by VisualSonics.

Acknowledgments—This work was supported in part by NIH grants R01CA111289 and R21HD061896 and by gift funds from Gammex, Inc.

REFERENCES

- Anderson ME, Soo MSC, Trahey GE. In vivo breast tissue backscatter measurements with 7.5- and 10-MHz transducers. *Ultrasound Med Biol* 2001;27:75–81.
- Bloomfield PE, Lo W-J, Lewin PA. Experimental study of the acoustical properties of polymers utilized to construct PVDF ultrasonic transducers and the acousto-electric properties of PVDF and P(VDF/TrFE) films. *IEEE Trans Ultrason Ferroelectr Freq Control* 2000;47:1397–1405.
- Del Grosso VA, Mader CW. Speed of sound in pure water. *J Acoust Soc Am* 1972;52:1442–1446.
- Ford RD. Introduction to acoustics. Amsterdam: Elsevier; 1971:75–77.
- Foster FS, Pavlin CJ, Christopher DA, Turnbull TH. Advances in ultrasound biomicroscopy. *Ultrasound Med Biol* 2000;26:1–27.
- Kaye GWC, Laby TH, (eds). Tables of physical and chemical constants. 14th ed. New York: Longman; 1973. p. 69.
- Kinsler EK, Frey AR, Coppens AB, Sanders JV. Fundamentals of acoustics. 3rd ed. New York: John Wiley; 1982:126.
- Kremkau FW, Barnes RW, McGraw CP. Ultrasonic attenuation and propagation speed in normal human brain. *J Acoust Soc Am* 1981;70:29–38.
- Labyed Y, Bigelow TA, McFarlin BL. Estimate of the attenuation coefficient using a clinical array transducer for the detection of cervical ripening in human pregnancy. *Ultrasonics* 2011;51:34–39.
- Lu ZF, Zagzebski JA, Lee FT. Ultrasound backscatter and attenuation in human liver with diffuse disease. *Ultrasound Med Biol* 1999;25:1047–1054.
- Madsen EL, Frank GR, McCormick MM, Deaner ME, Stiles TA. Anechoic sphere phantoms for estimating 3-D resolution of very-high-frequency ultrasound scanners. *IEEE Trans Ultrason Ferroelectr Freq Control* 2010;57:2284–2292.
- McCormick MM. Carotid Plaque Characterization with Medical Ultrasound. PhD Thesis 2011.
- McFarlin BL, Bigelow TA, Labyed Y, O'Brien WD Jr, Oelze ML. Ultrasonic attenuation estimation of the pregnant cervix: a preliminary report. *Ultrasound Obstet Gynecol* 2010;36:218–225.
- O'Donnell M, Jaynes ET, Miller JG. Kramers-Kronig relationship between ultrasonic attenuation and phase velocity. *J Acoust Soc Am* 1981;69:696–701.
- Raju BI, Srinivasan MA. High frequency ultrasonic attenuation and backscatter coefficients of in vivo normal human dermis and subcutaneous fat. *Ultrasound Med Biol* 2001;27:1543–1556.
- Shi H, Tu H, Dempsey RJ, Varghese T. Ultrasonic attenuation estimation in small plaque samples using a power difference method. *Ultrason Imaging* 2007;29:15–30.
- Stiles TA, Madsen EL, Frank GR. An exosimetry system using tissue-mimicking liquid. *Ultrasound Med Biol* 2008;34:123–136.
- Strowitzki M, Brand S, Jenderka K. Ultrasonic radiofrequency spectrum analysis of normal brain tissue. *Ultrasound Med Biol* 2007;33:522–529.

- Taylor JR. An introduction to error analysis, the study of uncertainties in physical measurements. 2nd edition. Sausalito, CA: University Science Books; 1997:107.
- Wear KA, Stiles TA, Frank GR, Madsen EL, Cheng F, Feleppa EJ, Hall CS, Kim BS, Lee P, O'Brien WD Jr, Oelze ML, Raju BI, Shung KK, Wilson TA, Yuan JR. Interlaboratory comparison of ultrasonic backscatter coefficient measurements from 2 to 9 MHz. *J Ultrasound Med* 2005;24:1235–1250.
- Yao LX, Zagzebski JA, Madsen EL. Backscatter coefficient measurements using a reference phantom to extract depth-dependent instrumentation factors. *Ultrasonic Imaging* 1990;12:58–70.

APPENDIX

Following is the derivation of the correction factor T_{tot} in eqn (2). The amplitude transmission coefficient from medium 1 to medium 2 for normal incidence is $T_{1 \rightarrow 2} = 2r_2/(r_1 + r_2)$, where r_1 and r_2 are the acoustic impedances of media 1 and 2 (Kinsler *et al.* 1982), and that for transmission from medium 2 to medium 1 is $T_{2 \rightarrow 1} = 2r_1/(r_1 + r_2)$. Thus, when the part of the pulse addressed involves no reverberations between two parallel interfaces with medium 2 between medium 1 on either side, we have $T_{\text{tot}} = T_{1 \rightarrow 2} T_{2 \rightarrow 1} = 4r_1 r_2 / (r_1 + r_2)^2$. In our case, medium 2 is TPX and medium 1 is water (w), and the relation becomes $T_{\text{tot}} = 4r_w r_{\text{TPX}} / (r_w + r_{\text{TPX}})^2$.